International Journal of Innovative Engineering Applications

Journal homepage: https://dergipark.org.tr/ijiea

FREE VIBRATION ANALYSIS OF LAMINATED COMPOSITE BEAMS CONSIDERING DELAMINATION EFFECTS USING GENERALIZED LAMINATION THEORY

Sebahat Şimşek*[1]

[1]Department of Civil Engineering, Faculty of Engineering, Karadeniz Technical University, Trabzon, Turkey

Abstract

Original scientific paper

Laminated composites exhibit highly complex damage mechanisms. One of the most critical failure modes is delamination, which refers to the separation between adjacent layers and can lead to significant reductions in structural stiffness. A major challenge associated with delamination is its invisibility on the material surface, making visual detection difficult. Although vibration-based damage detection methods offer a promising solution for identifying delamination, the effectiveness of such approaches relies on the availability of an accurate numerical model that can capture the behavior of delaminated structures. This study focuses on the modeling of delamination damage in laminated composite beams and the investigation of their free vibration behavior through the generalized lamination theory and finite element analysis. The displacement field within each lamina is assumed to vary linearly based on Lagrange polynomials, while terms accounting for interlayer sliding and separation caused by delamination are explicitly included. The governing equations of motion are derived using Hamilton's principle, and the corresponding mass and stiffness matrices are formulated using the Galerkin method. The influence of delamination length and position on the natural frequencies and mode shapes is examined under various boundary conditions and laminate stacking sequences. The results are compared with existing studies in the literature to validate the accuracy of the proposed model. Additionally, three-dimensional finite element models are developed using ANSYS® software to perform a comparative analysis. Two different modeling strategies for the delaminated interfaces are considered: in the first, nodes on the delaminated surfaces are allowed to move independently; in the second, contact elements are used to constrain the relative motion between layers. The impact of these two modeling approaches on the simulation results is evaluated in detail.

Keywords: *Delamination, free vibration, finite element method, generalized lamination theory, layered composite beam.*

1 Introduction

The rapid advancement in technology and industrial innovation has significantly increased the demand for advanced structural materials characterized by high strength-to-weight ratios, enhanced durability, corrosion resistance, favorable thermal properties, and ease of manufacturing. Composite materials, particularly laminated composites, fulfill these criteria and have consequently become indispensable in various engineering fields, including aerospace, automotive, marine, civil infrastructure, energy production, and mechanical systems.

Despite their numerous benefits, laminated composite structures exhibit unique damage mechanisms due to their heterogeneous and anisotropic nature. Unlike conventional isotropic materials where damage typically manifests visibly as surface cracks, laminated composites predominantly experience internal damage, such as matrix cracking, fiber fractures, and especially delamination—the separation of adjacent layers—before reaching catastrophic structural failure [1], [2]. Such internal damage might initially remain undetected yet significantly degrade the structural integrity, stiffness, and overall load-bearing capacity of composite structures.

Delamination is recognized as a critical failure mechanism in laminated composites, often initiated by interlaminar stress concentrations arising from fatigue loading, transverse impacts, or complex loading conditions [1], [3]. Accurately predicting the onset and progression of delamination is essential for ensuring structural safety and integrity. Consequently, substantial research effort has been dedicated to developing robust and precise numerical modeling approaches to simulate and predict delamination phenomena.

The Finite Element Method (FEM) remains one of the most widely employed numerical tools for analyzing complex damage phenomena, including delamination in laminated composites. The accuracy and reliability of FEM simulations are highly influenced by the underlying theoretical framework and the assumptions utilized to represent the material and structural behavior [4]. To this end, several advanced theories have been proposed, including the Equivalent Single Layer (ESL) theory [5]–[7], the Layerwise theory [7]–[9], the Zig-Zag theory [10]–[13], and the Three-Dimensional Elasticity theory [14], [15].

While ESL theories offer computational simplicity and efficiency, they are inadequate for accurately capturing the complex interlaminar stress fields,

*Corresponding author.

E-mail address: sebahatkaraca@ktu.edu.tr (S. Şimşek)

Received 06 May 2025; Received in revised form 30 May 2025; Accepted 03 June 2025

 Doi: https://doi.org/10.46460/ijiea.1693283

especially in thick laminates or when detailed local damage analyses are required. In contrast, Layerwise theories overcome these limitations by independently modeling each laminate layer, providing detailed descriptions of displacement and stress distributions through the laminate thickness [16], [17]. Recent developments have enhanced Layerwise theory further, notably the Carrera Unified Formulation (CUF), which allows for flexible, high-order expansions to accurately capture multilayered composite behavior [18], [19]. Additionally, integration of advanced numerical methods, such as modified spectral collocation approaches, has significantly improved the predictive capability of Layerwise theories, particularly in complex boundary condition scenarios [17].

Despite these theoretical advancements, a notable gap remains in comprehensive comparative studies between simplified LW-based analytical approaches and fully three-dimensional FEM solutions under delamination conditions, particularly concerning free vibration analyses. Addressing this gap is essential to establish the practical reliability and limitations of simpler analytical frameworks in predicting dynamic structural responses.

Motivated by this need, the present study systematically investigates the free vibration characteristics of laminated composite beams subjected to various delamination scenarios. The analytical model employed is based on Reddy's delaminated beam theory, utilizing linear Lagrange shape functions to represent inter-layer displacement behavior accurately. The model explicitly incorporates interlaminar slip and normal separation effects associated with delamination. The governing equations of motion are derived using Hamilton's principle, while the mass and stiffness matrices are constructed through the Galerkin procedure.

To validate the developed analytical formulation, comparative numerical simulations are conducted using the commercial FE software ANSYS®. The three-dimensional FEM employs SOLID185 elements, modeling delaminated interfaces with two distinct methods: one permitting free separation between layers and another employing contact elements to replicate realistic ply interactions. The resulting free vibration responses under varying delamination configurations are extensively analyzed and compared.

2 Generalized Lamination Theory

2.1 Kinematic Relations and Constitutive Equations

Figure 1 illustrates a schematic view of a composite beam experiencing delamination. In this figure, x_0, z_i and d represent the delamination midpoint's distance from the origin, the interface location of delamination, and the total length of the delamination, respectively. The beam's displacement field is formulated by Equation (1) [20]:

$$\begin{aligned} u(x,z,t) &= u^{LWT}(x,z,t) + u^{DEL}(x,z,t) \\ v(x,z,t) &= 0 \\ w(x,z,t) &= w^{LWT}(x,z,t) + w^{DEL}(x,z,t) \end{aligned} \tag{1}$$

where u^{LWT} and w^{LWT} denote displacements along the longitudinal (x) and transverse (z) axes. The terms u^{DEL} and w^{DEL} define the relative in-plane shear and out-of-plane separation displacements at the delaminated interface. These are further detailed in Equation (2):

$$\begin{aligned} u^{LWT}(x,z,t) &= \sum_{I=1}^{N} U_I(x,t)\Phi^I(z), \\ w^{LWT}(x,z,t) &= \sum_{i=1}^{N} W_I(x,t)\Phi^I(z), \\ u^{DEL}(x,z,t) &= \sum_{I=1}^{ND} {}^{D}U_I(x,t)H^I(z), \\ w^{DEL}(x,z,t) &= \sum_{i=1}^{ND} {}^{D}W_I(x,t)H^I(z) \end{aligned} \tag{2}$$

In this context, *ND* indicates the number of delaminated regions within the beam. The Heaviside unit step function, defined in Equation (3), captures the discontinuity due to delamination:

$$H^I(z) = \hat{H}^I(z - z_i) = \begin{cases} 1 & z \geq z_i \\ 0 & z < z_i \end{cases} \tag{3}$$

Within these equations, z_i signifies the interface location where delamination occurs, and the functions ${}^{D}U_I$ and ${}^{D}W_I$ represent shear slip and normal separation between the respective layers.

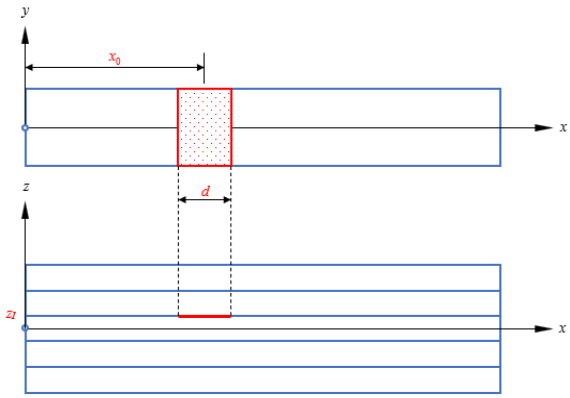

Figure 1. Geometry and coordinate axes of a delaminated beam.

Using the displacement relations provided in Equations (1) and (2), the corresponding strain-displacement relationships are derived:

$$\begin{aligned} \varepsilon_{xx} &= \sum_{I=1}^{N} \frac{dU_I}{dx}\Phi^I + \sum_{I=1}^{ND} \frac{d\,{}^{D}U_I}{dx}H^I, \\ \varepsilon_{yy} &= \gamma_{xy} = \gamma_{yz} = 0, \\ \varepsilon_{zz} &= \sum_{I=1}^{N} W_I \frac{d\Phi^I}{dz}, \\ \gamma_{xz} &= \sum_{I=1}^{N} \left(U_I \frac{\partial \Phi^I}{\partial z} + \frac{\partial W_I}{\partial x}\Phi^I \right) + \sum_{I=1}^{ND} \frac{\partial\, {}^{D}W_I}{\partial x} H^I \end{aligned} \tag{4}$$

$$\begin{Bmatrix}\sigma_{xx}\\ \sigma_{zz}\\ \tau_{xz}\end{Bmatrix}^k = \begin{bmatrix}\tilde{C}_{11} & \tilde{C}_{13} & 0\\ \tilde{C}_{31} & \tilde{C}_{33} & 0\\ 0 & 0 & \tilde{C}_{55}\end{bmatrix}^k \begin{Bmatrix}\varepsilon_{xx}\\ \varepsilon_{zz}\\ \gamma_{xz}\end{Bmatrix}^k \tag{5}$$

Here, the coefficients $\tilde{C}_{ij}^k$ represent the transformed reduced stiffness values for each individual layer [20].

2.2 Equations of Motion

Let δT represent virtual kinetic energy, δU virtual strain energy, and the virtual work by external forces. According to Hamilton's principle [15]:

$$\int_{t_1}^{t_2} \{\delta T - (\delta U + \delta V)\}\, dt = 0 \tag{6}$$

Since the current analysis addresses the beam's free vibration behavior, the term δV becomes zero. Inserting the respective energy formulations into Equation (6) and executing variational procedures leads to the governing equations of motion, expressed as:

3 Finite Element Model

3.1 Finite Element Model Based on the Generalized Lamination Theory

Figure 2 depicts the finite element representation of a beam containing an interfacial delamination. The displacement field within each FE is formulated as:

$$\begin{aligned} U_I(x,t) &= \sum_{j=1}^{2} U_I^j(t)\varphi_j(x),\\ W_I(x,t) &= \sum_{j=1}^{2} W_I^j(t)\varphi_j(x),\\ {}^D U_I(x,t) &= \sum_{j=1}^{2} {}^D U_I^j(t)\varphi_j(x),\\ {}^D W_I(x,t) &= \sum_{j=1}^{2} {}^D W_I^j(t)\varphi_j(x) \end{aligned} \tag{8}$$

In this expression, U_I, W_I, ${}^D U_I$ and ${}^D W_I$ are the generalized coordinates associated with the element's degrees of freedom. The interpolation functions φ_i are linear Lagrange polynomials applied for spatial discretization within the FE context. By substituting the displacement field described in Equation (8) into the motion equations obtained previously (Equation (7)), and subsequently applying the Galerkin method, the elemental FE equation is derived as:

$$M^e + \ddot{U}^e + K^e U^e \tag{9}$$

where, M^e and K^e denote the elemental mass and stiffness matrices, while U^e and $\ddot{U}^e$ represent the element displacement and acceleration vectors, respectively. These vectors are defined as follows:

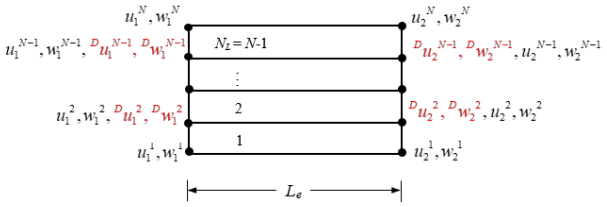

Figure 2. Finite element model with delamination.

$$\mathbf{M}^e = \begin{bmatrix}\mathbf{M}_{11}^{IJ} & \mathbf{0} & \mathbf{M}_{13}^{IJ} & \mathbf{0}\\ \mathbf{0} & \mathbf{M}_{22}^{IJ} & \mathbf{0} & \mathbf{M}_{24}^{IJ}\\ \mathbf{M}_{31}^{IJ} & \mathbf{0} & \mathbf{M}_{33}^{IJ} & \mathbf{0}\\ \mathbf{0} & \mathbf{M}_{42}^{IJ} & \mathbf{0} & \mathbf{M}_{44}^{IJ}\end{bmatrix},\quad \mathbf{K}^e = \begin{bmatrix}\mathbf{K}_{11}^{IJ} & \mathbf{K}_{12}^{IJ} & \mathbf{K}_{13}^{IJ} & \mathbf{K}_{14}^{IJ}\\ \mathbf{K}_{21}^{IJ} & \mathbf{K}_{22}^{IJ} & \mathbf{K}_{23}^{IJ} & \mathbf{K}_{24}^{IJ}\\ \mathbf{K}_{31}^{IJ} & \mathbf{K}_{32}^{IJ} & \mathbf{K}_{33}^{IJ} & \mathbf{0}\\ \mathbf{K}_{41}^{IJ} & \mathbf{K}_{42}^{IJ} & \mathbf{0} & \mathbf{K}_{44}^{IJ}\end{bmatrix},$$
$$\ddot{\mathbf{U}}^e = \begin{bmatrix}\ddot{\mathbf{U}}^J & \ddot{\mathbf{W}}^J & {}^D\ddot{\mathbf{U}}^J & {}^D\ddot{\mathbf{W}}^J\end{bmatrix}^T,\quad \mathbf{U}^e = \begin{bmatrix}\mathbf{U}^J & \mathbf{W}^J & {}^D\mathbf{U}^J & {}^D\mathbf{W}^J\end{bmatrix}^T \tag{10}$$

The evaluation of the submatrices within the global system requires integral expressions, which are provided by:

$$\begin{aligned} M_{11ij}^{IJ} &= M_{22ij}^{IJ} = \int_0^L \{I_1^{IJ}\varphi_i\varphi_j\}\,dx, \quad M_{13ij}^{IJ} = M_{24ij}^{IJ} = \int_0^L \{I_3^{IJ}\varphi_i\varphi_j\}\,dx,\\ M_{31ij}^{IJ} &= M_{42ij}^{IJ} = \int_0^L \{I_2^{IJ}\varphi_i\varphi_j\}\,dx, \quad M_{33ij}^{IJ} = M_{44ij}^{IJ} = \int_0^L \{I_4^{IJ}\varphi_i\varphi_j\}\,dx \end{aligned} \tag{11}$$

$$\begin{aligned} K_{11ij}^{IJ} &= \int_0^L \left\{A_{11}^{IJ}\frac{\partial\varphi_i}{\partial x}\frac{\partial\varphi_j}{\partial x} + \bar{A}_{55}^{IJ}\varphi_i\varphi_j\right\}dx,\\ K_{12ij}^{IJ} &= \int_0^L \left\{\tilde{A}_{13}^{IJ}\frac{\partial\varphi_i}{\partial x}\varphi_j + \bar{B}_{55}^{IJ}\varphi_i\frac{\partial\varphi_j}{\partial x}\right\}dx,\\ K_{13ij}^{IJ} &= \int_0^L \left\{{}^D A_{11}^{IJ}\frac{\partial\varphi_i}{\partial x}\frac{\partial\varphi_j}{\partial x}\right\}dx, \quad K_{14ij}^{IJ} = \int_0^L \left\{{}^D\bar{B}_{55}^{IJ}\varphi_i\frac{\partial\varphi_j}{\partial x}\right\}dx,\\ K_{21ij}^{IJ} &= \int_0^L \left\{\bar{B}_{55}^{JI}\frac{\partial\varphi_i}{\partial x}\varphi_j + \tilde{A}_{31}^{JI}\varphi_i\frac{\partial\varphi_j}{\partial x}\right\}dx,\\ K_{22ij}^{IJ} &= \int_0^L \left\{\bar{D}_{55}^{IJ}\frac{\partial\varphi_i}{\partial x}\frac{\partial\varphi_j}{\partial x} + \hat{A}_{33}^{IJ}\varphi_i\varphi_j\right\}dx,\\ K_{23ij}^{IJ} &= \int_0^L \left\{{}^D\tilde{A}_{31}^{JI}\varphi_i\frac{\partial\varphi_j}{\partial x}\right\}dx, \quad K_{24ij}^{IJ} = \int_0^L \left\{{}^D\bar{A}_{55}^{JI}\frac{\partial\varphi_i}{\partial x}\frac{\partial\varphi_j}{\partial x}\right\}dx,\\ K_{31ij}^{IJ} &= \int_0^L \left\{{}^D\tilde{A}_{11}^{IJ}\frac{\partial\varphi_i}{\partial x}\frac{\partial\varphi_j}{\partial x}\right\}dx, \quad K_{32ij}^{IJ} = \int_0^L \left\{{}^D\tilde{A}_{13}^{IJ}\frac{\partial\varphi_i}{\partial x}\varphi_j\right\}dx,\\ K_{33ij}^{IJ} &= \int_0^L \left\{{}^D\bar{\bar{A}}_{11}^{IJ}\frac{\partial\varphi_i}{\partial x}\frac{\partial\varphi_j}{\partial x}\right\}dx, \quad K_{41ij}^{IJ} = \int_0^L \left\{{}^D\bar{B}_{55}^{JI}\frac{\partial\varphi_i}{\partial x}\varphi_j\right\}dx,\\ K_{42ij}^{IJ} &= \int_0^L \left\{{}^D\bar{A}_{55}^{JI}\frac{\partial\varphi_i}{\partial x}\frac{\partial\varphi_j}{\partial x}\right\}dx, \quad K_{44ij}^{IJ} = \int_0^L \left\{{}^D\bar{\bar{A}}_{55}^{IJ}\frac{\partial\varphi_i}{\partial x}\frac{\partial\varphi_j}{\partial x}\right\}dx \end{aligned} \tag{12}$$

Within these formulations, the matrices *A*, *B* and terms correspond to the laminate's extensional stiffness, coupling stiffness, and bending stiffness matrices, respectively, as established in composite lamination theory [21].

3.2 ANSYS® Finite Element Model

To validate the analytical results derived from the generalized lamination theory, a comprehensive three-dimensional FE model of the delaminated composite beam was developed using ANSYS 16.0, a widely utilized commercial FE analysis software.

For the structural discretization of the laminated composite beam, the SOLID185 element type was employed. SOLID185 is an 8-node hexahedral element capable of modeling nonlinear material behavior, large deformations, and strain-based geometric nonlinearity. Each node has three translational degrees of freedom (UX,

UY, UZ), allowing accurate simulation of deformation in 3D space. To capture the thorough-thickness behavior of the laminated structure with sufficient fidelity, one element per layer was used across the thickness direction. This modeling approach enabled precise characterization of interlaminar stress distributions and deformation gradients, which are particularly significant in the presence of delamination.

The laminate stacking sequence, ply orientation angles, and orthotropic material properties were defined using the SHELL SECTION assignment for layered solids. This ANSYS feature allows users to assign varying fiber orientations, elastic properties, and thicknesses to each ply within a single layered volume, thereby facilitating accurate representation of composite layups without requiring separate meshing for each ply.

A mesh convergence study was performed to determine the optimal element size that balances accuracy with computational cost. Several mesh configurations were analyzed, with natural frequency convergence used as the primary assessment metric. Following this parametric analysis, a refined mesh configuration comprising 1752 elements and 1664 nodes was adopted for all simulations, ensuring consistency across models while maintaining numerical efficiency.

In the FE model, interlaminar continuity was enforced across intact interfaces by coupling the degrees of freedom (DOFs) between nodes of adjacent plies. This constraint condition ensures that no relative displacement occurs in undamaged regions, accurately simulating the perfect bonding assumption typical in composite theory. Conversely, at delaminated interfaces, the nodes were left uncoupled to allow independent movement, thereby replicating the mechanical discontinuity caused by delamination.

To model the delaminated interface behavior, two distinct strategies were implemented:

First Strategy – Free Node Separation: In this simplified method, nodes on opposing delaminated surfaces were left entirely unconstrained. This approach permits full relative motion between the delaminated plies in all spatial directions, offering computational simplicity. However, such an assumption may yield non-physical results under dynamic loading, including excessive separation or even interpenetration of layers, particularly during out-of-plane vibration responses (see Figure 3(a)). Consequently, this method is primarily used for preliminary evaluations or when qualitative behavior is of interest.

Second Strategy – Contact-Based Delamination Modeling: A more realistic and physically robust approach was implemented using contact elements, specifically CONTAC173 and TARGE170. These allow accurate modeling of interface interactions by defining surface-to-surface contact behavior.

TARGE170 represents the target surface and is usually assigned to the stiffer body or underlying layer. CONTAC173 is designated as the contact surface and is applied to the deformable body, enabling interaction with the target during loading.

This strategy permits the model to replicate the asymmetric behavior of delaminated interfaces:

During compressive loading, contact elements transfer normal forces between plies, effectively preventing interpenetration and ensuring realistic mechanical response.

Under tensile conditions, the contact pair automatically deactivates, allowing the delaminated surfaces to separate freely. This behavior reflects the actual physical mechanism of delamination propagation and recovery (see Figure 3(b)).

The contact parameters, including normal stiffness, frictional properties (if applicable), and penetration tolerance, were carefully selected to avoid numerical instabilities while preserving solution accuracy. This contact-based approach significantly enhances the realism of the FE simulations, particularly for vibration and stability analyses of delaminated composite structures.

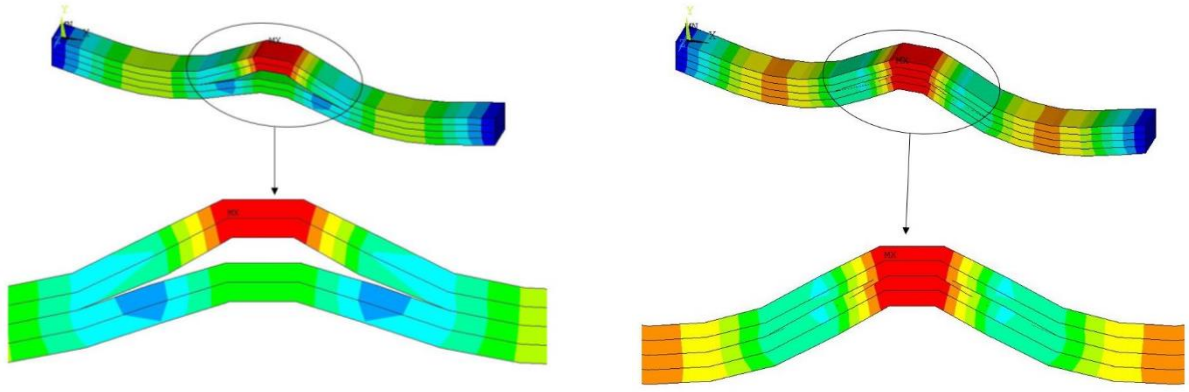

(a) (b)

Figure 3. FE models of delaminated beams created in ANSYS®: (a) without contact elements, (b) with contact elements.

4 Results and Discussion

In order to obtain sufficiently accurate results in the finite element analyses, a mesh convergence study was first conducted. For this purpose, a laminated composite beam with a length of L = 300 mm, width b = 20 mm, and height h = 20 mm was considered. The beam is made of AS3501/6 graphite-epoxy material. The material properties are as follows: E_1 = 144.9 GPa, E_2 = 9.65 GPa, G_{12} = G_{13} = 4.14 GPa, G_{23} = 3.45 GPa, ν = 0.3, and ρ = 1389.23 kg/m³ [22]. Table 1 presents the variation of the first three dimensionless natural frequencies of a clamped–clamped undamaged $(0/90)_2$ beam with respect

to the number of elements. The natural frequencies are expressed in a nondimensional form. As observed, the dimensionless natural frequencies decrease rapidly and converge toward a constant value as the number of elements increases. Based on the table, it is concluded that using N = 80 elements in the finite element analyses is sufficient.

To verify the accuracy of the natural frequencies obtained using the generalized lamination theory and to validate the results for potential damage detection applications, a comparison with existing literature results was performed. Specifically, the non-dimensionalized natural frequencies of a symmetrically delaminated isotropic fixed-fixed beam were considered, based on the study in [23]. The dimensionless frequency parameter Ω was defined as follows:

$$\Omega^2 = \left(\frac{\rho_0 A_0}{E_0 I_0} \right) L_0^4 \omega^2 \tag{13}$$

where ρ_0 is the material density,, A_0 is the cross-sectional area, E_0 is the Young's modulus, I_0 is the second moment of area (moment of inertia), L_0 is the total beam length, and is the angular frequency.

Table 2 presents a comparative summary of the dimensionless natural frequencies obtained in the present study alongside those reported in [23]. The results demonstrate excellent agreement, confirming the validity of the present FE model and analytical approach.

The results clearly show a very strong correlation between the natural frequencies obtained in the present study and those reported in [23] who employed an analytical solution. Particularly for small delamination lengths (a / $L \leq 0.1$), the dimensionless frequencies are nearly identical, indicating the robustness of the modeling approach for slight damage scenarios.

When the results are evaluated internally, as the relative length of the delamination (a / L) increases, a progressive decrease in the natural frequencies is observed, with the higher modes being particularly more affected. While the first natural frequency Ω_1 exhibits a relatively slower reduction, the second and third modes demonstrate greater sensitivity to the presence and growth of delamination. This behavior suggests that higher vibration modes are more effective indicators of delamination damage. Moreover, when the delamination length exceeds a / $L \geq 0.6$, the frequency reduction becomes significantly more pronounced, reflecting substantial stiffness degradation and a corresponding loss of structural integrity.

Table 1. Finite element convergence analysis.

Number of Elements	Natural Frequencies		
	Ω_1	Ω_2	Ω_3
10	3.9395	9.5608	16.8382
20	3.7246	8.8667	15.2230
30	3.6833	8.7352	14.9225
40	3.6687	8.6886	14.8168
60	3.6581	8.6551	15.7410
80	**3.6543**	**8.6433**	**14.7143**
100	3.6526	8.6378	15.7019

Table 2. Non-dimensional natural frequencies of an isotropic fixed-fixed beam with mid-plane delamination.

a / L	Present Study			Analytical [23]		
	Ω_1	Ω_2	Ω_3	Ω_1	Ω_2	Ω_3
0.00	22.6131	61.1880	117.1458	22.39	61.67	120.91
0.05	22.6131	61.1090	117.1447	22.37	61.53	120.90
0.10	22.6126	60.5399	117.1012	22.37	60.76	120.81
0.20	22.5984	56.7449	115.7720	22.35	55.97	118.76
0.30	22.5032	50.7074	108.8308	22.23	49.00	109.04
0.40	22.1713	45.8342	96.1191	21.83	43.87	93.57
0.50	21.3842	43.3365	85.5149	20.88	41.45	82.29
0.60	20.0055	42.7007	80.5521	19.29	40.93	77.64
0.70	18.1395	42.5913	79.7721	17.23	40.72	77.05
0.80	16.0652	41.2531	78.7290	15.05	39.01	75.33
0.90	14.0357	37.9362	73.5082	13.00	69.17	68.84
0.99	12.4029	34.0117	66.2261	11.36	61.36	61.36

To validate the finite element model, a cantilever composite beam with a $(0/-45/45/90)_s$ stacking sequence was considered. The beam has a length of L = 244 mm, while its height and width are given in Table 3. The material properties are as follows: E_1 = 92.5 GPa, E_2 = 8.04 GPa, $G_{12} = G_{13}$ = 2.88 GPa, G_{23} = 2.80 GPa, ν = 0.33, and ρ = 1429.0 kg/m³ [24]. The damage scenarios considered are listed in Table 3. Table 4 presents the first five natural frequencies (Hz) of the beam for both the undamaged case and four different damage scenarios. The results of this study were compared with the experimental data reported in [24]. As can be seen, the results are in good agreement with each other.

Table 3. Dimensions and damage scenarios for cantilever composite beams with (0/−45/45/90)s lay-up [24].

Model	Width (mm)	Thickness (mm)	Delaminated Interface	Delamination Length (mm)	Distance from Support (mm)
Undamaged	19.18	2.27	-	-	-
Case 1	19.25	2.46	4	28	44.9
Case 2	19.09	2.66	3	31	45.3
Case 3	19.36	2.76	2	60.2	105.1
Case 4	18.98	2.69	1	34.5	43

Table 4. First five natural frequencies for undamaged and delaminated cantilever beams with (0/−45/45/90)s.

Method	f_1	f_2	f_3	f_4	f_5
Undamaged					
Present Study	40.6109	253.9843	708.9229	1382.971	2273.114
Zhang et al. (2014) [24]	40	248	698	1362	2244
Case 1					
Present Study	43.6278	266.5954	736.2754	1463.726	2418.190
Zhang et al. (2014) [24]	46	260	724	1482	2434
Case 2					
Present Study	46.88932	284.1747	780.3951	1555.483	2587.254
Zhang et al. (2014) [24]	50	286	792	1610	2636
Case 3					
Present Study	47.9252	295.0304	717.4321	1330.968	2286.246
Zhang et al. (2014) [24]	48	276	704	1434	2402
Case 4					
Present Study	47.4401	290.4456	799.5212	1576.927	2615.020
Zhang et al. (2014) [24]	44	290	804	1564	2665

Following the validation study, numerical results concerning the natural frequencies and mode shapes of a laminated composite beam under various delamination scenarios are presented. The beam considered has a $[0/90]_2$ stacking sequence, with both ends fixed, and equal layer thicknesses are assumed. The material properties for a single ply are taken as: E_1 = 144.9 GPa, E_2 = 9.65 GPa, $G_{12} = G_{13}$ = 4.14 GPa, G_{23} = 3.45 GPa, Poisson's ratio ν = 0.3 and density ρ = 1389.23 kg/m^3. The beam dimensions are considered as L/h =15, $b = h$ = 1 unit.

Table 5 summarizes the delamination scenarios considered in the analysis. In all cases, a single delamination is located at the mid-span of the beam. Variations in delamination position across different interfaces and changes in delamination length are investigated to assess their effects on the natural frequencies and mode shapes. In the first three scenarios (S1–S3), the delamination length is L/5, while in the last three scenarios (S4–S6), it is increased to L/3. In both sets, the delamination is positioned sequentially at different interlaminar interfaces.

Numerical results were obtained using a FE code developed in FORTRAN and compared against results obtained from a 3D FE model created in ANSYS®. In the ANSYS® simulations, contact elements were employed along delaminated surfaces to realistically capture opening and sliding effects between layers. It was observed that the inclusion of contact elements did not significantly alter the natural frequencies but affected the deformation patterns during vibration.

Table 5. Delamination scenarios considered in the analysis.

Damage Scenario	Variables describing delamination (see Figure 1)		
	Interface, z_I	Length, d	Midpoint, x_0
S1	1	L / 5	L / 2
S2	2	L / 5	L / 2
S3	3	L / 5	L / 2
S4	1	L / 3	L / 2
S5	2	L / 3	L / 2
S6	3	L / 3	L / 2

Table 6. First four natural frequencies (Hz) obtained from Reddy's Theory and ANSYS® for different delamination scenarios.

Damage Scenario	f_1		f_2		f_3		f_4	
	Reddy	ANSYS®	Reddy	ANSYS®	Reddy	ANSYS®	Reddy	ANSYS®
S1	2633.67	2667.07	5430.13	6366.64	10399.47	11019.80	12929.54	16151.90
S2	2632.64	2663.77	5409.83	5587.51	10342.91	10869.89	12914.37	13782.94
S3	2623.31	2663.76	6213.01	5595.65	11185.41	10869.93	14814.82	13785.87
S4	2579.53	2666.09	4542.21	6319.76	9005.38	10987.01	12460.03	15864.43
S5	2573.47	2617.85	4518.34	4651.17	9002.69	9559.01	12455.67	13295.84
S6	2308.58	2618.57	5911.20	4668.30	11015.27	9571.07	15670.04	13299.48

The first four natural frequencies obtained for each damage scenario are listed in Table 6, showing results from both Reddy's theory-based FE model and the ANSYS® simulations. It can be observed that the presence of delamination significantly affects the natural frequencies of the composite beam. An increase in delamination length leads to a noticeable reduction in the natural frequencies across all modes. Specifically, for

shorter delaminations (scenarios S1–S3 with $d = L/5$), the natural frequencies from both methods are relatively close, with only minor differences. However, as the delamination length increases to $L/3$ (scenarios S4–S6), the reduction in frequency becomes more pronounced, and the differences between the two approaches tend to increase, particularly for the third and fourth modes. This behavior can be attributed to the growing influence of localized stiffness degradation, which affects the dynamic response more severely at higher frequencies.

Figures 4 and 5 illustrate the first four bending mode shapes for the beam with a delamination located at the second interface (Scenario S2), obtained using the proposed FE approach and ANSYS® simulations, respectively. In Figure 4, which corresponds to Reddy's theory-based model, discontinuities in the slope of the mode shapes are clearly visible at the start and end points of the delamination, indicating the localized stiffness reduction. These discontinuities are more pronounced in higher modes, consistent with the greater sensitivity of higher modes to local defects.

In contrast, Figure 5, showing the ANSYS® results, reveals additional physical phenomena. Relative sliding between the separated layers is clearly observed during vibration, a behavior captured due to the use of contact elements. While separation (opening) between the layers is less evident in lower modes, it becomes noticeable in the fourth mode, as the deformation becomes sufficiently large to induce contact opening. This observation confirms that the proposed numerical approach accurately captures key deformation characteristics while maintaining computational efficiency.

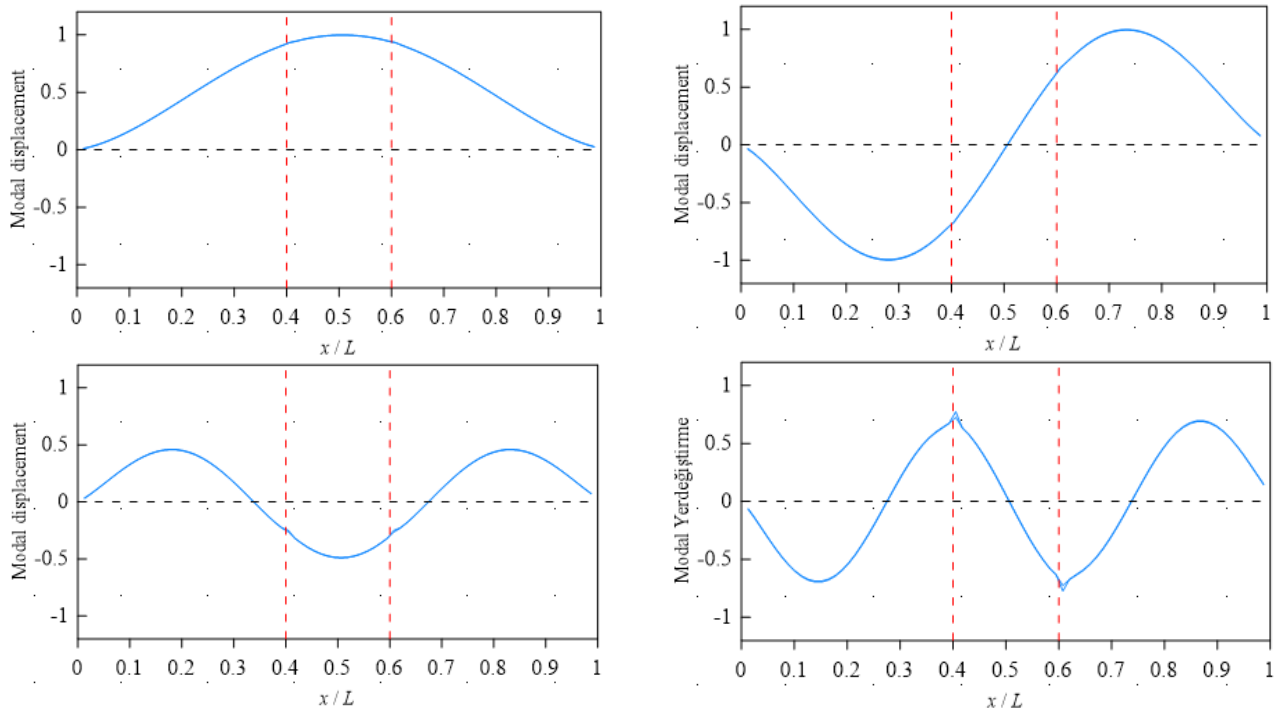

Figure 4. First four mode shapes of the fixed-fixed laminated composite beam obtained from the FE model based on Reddy's Theory (Scenario S2).

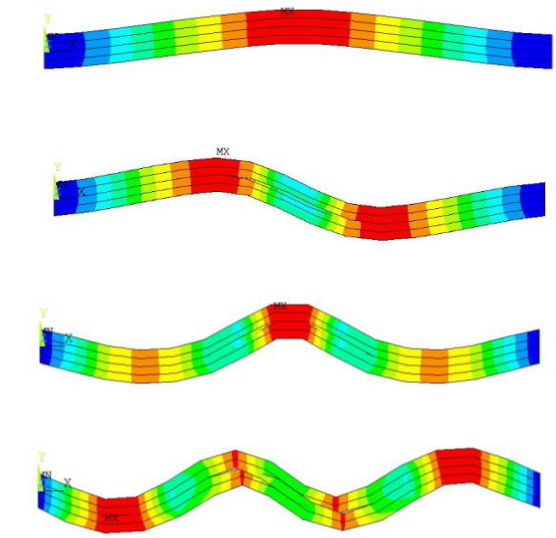

Figure 5. First four mode shapes of the fixed-fixed laminated composite beam obtained from ANSYS® Simulations (Scenario S2).

5 Conclusions

This study examined the free vibration behavior of laminated composite beams under various delamination scenarios using an FE formulation based on Reddy's delaminated beam theory. The displacement field within each ply was approximated by linear Lagrange polynomials, and interlaminar sliding and separation due to delamination, along with Poisson's effects, were considered. Equations of motion were derived via Hamilton's principle, and FE matrices were constructed using the Galerkin method.

Validation was performed against analytical results and three-dimensional FE simulations conducted using ANSYS®. The developed model exhibited excellent agreement with analytical solutions, particularly for smaller delamination, and maintained consistency as delamination length increased. ANSYS® simulations with SOLID185 elements employed both free-separation and contact-element modeling approaches.

- Increasing delamination length significantly reduces natural frequencies, highlighting the sensitivity of dynamic response to structural damage.
- Reddy's theory-based FE model efficiently simplifies the three-dimensional problem into a two-dimensional approach, achieving accurate predictions with lower computational effort.
- The developed model demonstrates strong agreement with both analytical and comprehensive 3D numerical solutions, confirming its accuracy and reliability.
- This approach provides a flexible and computationally efficient tool suitable for vibration-based damage detection in laminated composite structures.

Overall, the proposed FE methodology effectively captures delamination effects and represents a reliable approach for dynamic structural analyses of laminated composite beams.

Acknowledgments

The author would like to express their sincere gratitude to Prof. Volkan Kahya for his valuable comments in preparation of this work.

Declaration

Ethics committee approval is not required.

References

[1] Ghobadi, A. (2017). Common type of damages in composites and their inspections. *World Journal of Mechanics, 7*(2), 24–33.

[2] Li, D. (2021). Layerwise theories of laminated composite structures and their applications: A review. *Archives of Computational Methods in Engineering, 28*, 577–600.

[3] Torabi, K., Shariati-Nia, M., & Heidari-Rarani, M. (2016). Experimental and theoretical investigation on transverse vibration of delaminated cross-ply composite beams. *International Journal of Mechanical Sciences, 115–116*, 1–11.

[4] Della, C. N., & Shu, D. (2007). Vibration of delaminated composite laminates: A review. *Applied Mechanics Reviews, 60*(1), 1.

[5] Goyal, V. K., & Kapania, R. K. (2007). A shear-deformable beam element for the analysis of laminated composites. *Finite Elements in Analysis and Design, 43*(6–7), 463–477.

[6] Aguiar, R. M., Moleiro, F., & Mota Soares, C. M. M. (2012). Assessment of mixed and displacement-based models for static analysis of composite beams of different cross-sections. *Composite Structures, 94*(2), 601–616.

[7] Sayyad, A. S., & Ghugal, Y. M. (2017). Bending, buckling and free vibration of laminated composite and sandwich beams: A critical review of literature. *Composite Structures, 171*, 486–504.

[8] Hajianmaleki, M., & Qatu, M. S. (2013). Vibrations of straight and curved composite beams: A review. *Composite Structures, 100*, 218–232.

[9] Li, D. (2020). Layerwise theories of laminated composite structures and their applications: A review. *Archives of Computational Methods in Engineering, 1*(0123456789), 3.

[10] Lansing, E., & Lansing, E. (1999). C^0 zig-zag finite element for analysis of laminated composite beams. *Journal of Engineering Mechanics, 125*(3), 323–330.

[11] Zhen, W., & Wanji, C. (2008). An assessment of several displacement-based theories for the vibration and stability analysis of laminated composite and sandwich beams. *Composite Structures, 84*(4), 337–349.

[12] Khan, A. A., Alam, M. N., & Wajid, M. (2016). Finite element modelling for static and free vibration response of functionally graded beam. *Latin American Journal of Solids and Structures, 13*(4), 690–714.

[13] Filippi, M., & Carrera, E. (2016). Bending and vibrations analyses of laminated beams by using a zig-zag-layer-wise theory. *Composites Part B: Engineering, 98*, 269–280.

[14] Chen, W. Q., Lv, C. F., & Bian, Z. G. (2003). Elasticity solution for free vibration of laminated beams. *Composite Structures, 62*(1), 75–82.

[15] Kant, T., Gupta, A. B., Pendhari, S. S., & Desai, Y. M. (2008). Elasticity solution for cross-ply composite and sandwich laminates. *Composite Structures, 83*(1), 13–24.

[16] Liew, K. M., Pan, Z. Z., & Zhang, L. W. (2019). An overview of layerwise theories for composite laminates and structures: Development, numerical implementation and application. *Composite Structures, 216*, 240–259.

[17] Ji, M., Sekiguchi, Y., Naito, M., & Sato, C. (2025). A modified spectral collocation method for vibration of sandwich beams based on a higher-order layer-wise beam theory. *Thin-Walled Structures, 209*, Article 112949.

[18] Filippi, M., Giusa, D., Pagani, A., Zappino, E., & Carrera, E. (2020). Assessment of classical, advanced, and layer-wise theories for the vibration of rotating composite anisotropic blades. *Composite Structures, 245*, Article 112315.

[19] Augello, R., Carrera, E., & Saputo, S. (2025). Component-Wise measure of elastic energy contributions in laminated composite beams. *Composite Structures, 355*, Article 118842.

[20] Reddy, J. N. (2003). *Mechanics of laminated composite plates and shells: Theory and analysis* (2nd ed.). CRC Press/Balkema.

[21] Na, W. J. (2008). *Damage analysis of laminated composite beams under bending loads using the layer-wise theory* [Doctoral dissertation, Texas A&M University].

[22] Dinh-Cong, D., Vo-Duy, T., Nguyen-Minh, N., Ho-Huu, V., & Nguyen-Thoi, T. (2017). A two-stage assessment method using damage locating vector method and differential evolution algorithm for damage identification of cross-ply laminated composite beams. *Advances in Structural Engineering, 20*(12), 1807–1827.

[23] Wang, J. T. S., Liu, Y. Y., & Gibby, J. A. (1982). Vibrations of split beams. *Journal of Sound and Vibration, 84*(4), 491–502.

[24] Zhang, Z., Shankar, K., Morozov, E. V., & Tahtali, M. (2016). Vibration-based delamination detection in composite beams through frequency changes. *Journal of Vibration and Control, 22*(2), 496–512.